Journal of Materials Chemistry B

Accepted Manuscript

ROYAL SOCIETY OF CHEMISTRY

www.rsc.org/materialsB

Investigating the Potential of Human Placental Derived Extracellular Matrix Sponges Coupled with Amniotic Membrane-Derived Stem Cells for Osteochondral Tissue Engineering

Arun Prabhu Rameshbabu[Ψ], Paulomi Ghosh[Ψ], Elavarasan Subramani[Y], Kamakshi Bankoti[Ψ], Kausik Kapat[Ψ], Sayanti Datta[Ψ], Priti Prasana Maity[Ψ], Bhuvaneshwaran Subramanian[Ψ], Sabyasachi Roy[‡], Koel Chaudhury[Y] and Santanu Dhara[Ψ*]

[Ψ] Biomaterials and Tissue Engineering Laboratory

School of Medical Science and Technology

Indian Institute of Technology Kharagpur

Kharagpur – 721302, India

[Y] Reproductive Health Lab

School of Medical Science and Technology

Indian Institute of Technology Kharagpur

Kharagpur – 721302, India

[‡] Department of Gynaecology,

Midnapore Medical College,

Paschim Medinipur – 721101, India

[*]Corresponding author

Dr. Santanu Dhara

E-mail: sdhara@smst.iitkgp.ernet.in

Abstract

Osteochondral injuries are challenging to repair due to its complex tissue anatomy and restricted self-repairing ability associated with limited blood supply. Osteochondral tissue engineering implicates important clinical aspect in management and treatment of cartilage and underlying bone. In the present study, we fabricated a human placental derived extracellular matrix sponges (PEMS) for repair of osteochondral tissue through decellularization process. There was no significant cellular components present in PEMS and was proved by hematoxylin & eosin/DAPI staining, DNA quantification and agarose gel electrophoresis to validate the extent of decellularization. Also no significant alterations to the collagen and glycosaminoglycan (native extracellular matrix) content of PEMS was observed. PEMS *in vitro* provided a non-cytotoxic and bioactive cues rich environment for the human amniotic membrane derived stem cells (HAMSCs) to proliferate and differentiate into chondrogenic and osteogenic lineage under induction. Histological analysis of PEMS subcutaneously implanted after 28 days demonstrated no severe immune response in the host and supported the formation of blood vessel. To assess the osteochondral tissue repair ability of PEMS, cell free PEMS (CFP) and cell seeded PEMS (CSP) were implanted at osteochondral defect sites in a rabbit model. From histological scores it is evident that the defects filled with CSP was found to support superior osteochondral regeneration compared to CFP and empty defects (ED) after 60 days of implantation. In summary, a naturally derived biocompatible scaffold composed of extracellular matrix from human placenta has been successfully developed for osteochondral tissue engineering.

1. INTRODUCTION

Repair of osteochondral defects requires simultaneous restoration of both cartilage and bone. Although bone healing process is faster, the major challenge lies with the limited regenerative ability of cartilage due to its multi-layered graded structure and limited supply of blood.[1] Once the hyaline cartilage sheath of the articulating joints is disrupted due to injury, autoimmune disorders or several other reasons, mechanically unstable fibrocartilage is formed at the damaged site. The newly formed cartilage provides much lesser protection to the affected part of the subchondral bone since it is mechanically weaker than hyaline cartilage.[2] Hence, osteochondral lesions treatment is challenging to the orthopaedic surgeons. The current palliative treatment options for osteochondral defects are arthroscopic debridement and microfracture (for minor defects < 2.0 cm^2). Matrix-assisted autologous chondrocyte implantation and autologous chondrocyte implantation technologies are widely adopted for defects greater than 2.5 cm^2, since it helps in faster regeneration of hyaline cartilage. However, chondrocyte hypertrophy, apoptosis and necrosis are the major concerns.[3–6] In case of defect size more than ~ 4.0 cm^2, mosaicplasty is mostly preferred. But the major drawback of this method is the limited availability of donor tissues and the degradation of the newly grafted tissue during the post-operative period.[7] As a result, research on the potential alternative for osteochondral treatment are of great importance. In this context, tissue engineering holds enormous potential to treat osteochondral defects by using combinatorial approach involving scaffolds, stem cells/primary cells and growth factors.

The use of decellularized extracellular matrix (ECM) based scaffold from tissues and organs for restoring/repairing the damaged tissues or organs has increased in the recent past.[8] ECM derived from decellurization of placenta,[9] dermis,[10] cornea,[11] heart valve,[12] trachea,[13] skeletal muscle,[14] intervertebral disk,[15] liver,[16] bladder,[17] adipose tissue,[18] blood vessel,[19]

lung,[20] small intestinal submucosa,[21] bone,[22] and periosteum[23] etc. has shown promising results in creating a biologic scaffold capable of providing a favourable environment for survival, proliferation and differentiation of the resident cells (Stem cells/Primary cells). Interestingly, the plasticity of ECM enables it to be used as an universal scaffold for tissue engineering, regardless of the tissue origin from which it is derived,[24] since ECM is constantly remodelled in response to the metabolic activity of the resident cells. In this context, ECM derived from placental tissues is an attractive option and gained significant attention, as it contains abundant ECM components coupled with well-preserved endogenous bioactive molecules.[25] Also, these ECM and bioactive components have the ability to regulate the cellular activity better than any other synthetic biomaterials which makes it an appropriate choice as template for tissue engineering applications.[26] This has motivated us to fabricate a biologic scaffold from decellularized placenta for osteochondral tissue engineering. In the present study, we have developed a protocol to successfully obtain decellularized ECM sponges from human placenta (PEMS) with no significant alterations to the native extracellular matrix components and the bioactive molecules. We also evaluated the adhesion, proliferation and differentiation potential of HAMSCs towards chondrogenic and osteogenic lineage on this scaffold *in vitro*. PEMS was subcutaneously implanted into rabbits to study the host immune reaction *in vivo*. The cell free PEMS (CFP) and cell seeded PEMS (CSP) were implanted in the osteochondral defect of rabbits and assessed for their efficiency against empty defects (ED) towards accelerated osteochondral tissue repair.

2. MATERIALS AND METHODS

2.1. Decellularization of human placenta

Ten human placentas after caesarean deliveries were provided by Midnapore Medical College and Hospital after approval by the Institutional ethical committee for research

applications. Human placentas were decellularized using the protocol reported elsewhere with modifications.[27] Briefly, collected placentas were chopped into pieces and were washed with phosphate buffered saline (PBS) until they were free of blood components. The placenta was decellularized in a rotating vessel using 0.5% sodium dodecyl sulfate (SDS; Sigma-Aldrich, USA) with 200 mg/mL RNase (Sigma-Aldrich, USA), 0.2% DNase (2000 U; Sigma-Aldrich, USA), 0.05% trypsin/EDTA (Gibco, USA), 1 mM phenylmethylsulfonylfluoride (Sigma-Aldrich, USA), and 100 U/mL penicillin and 100 µg/mL streptomycin (Gibco, USA) at room temperature for 15 days. The process was carried out in sterile environment and the solution was changed every 2 days to avoid contamination and tissue degradation. The decellularized placentas was washed with PBS multiple times and stored at -80° for further use.

2.2. Histological analysis of native and decellularized placenta

Native placenta (NP) and decellularized placenta (DP) were fixed in 4% paraformaldehyde at room temperature for 24 h. Sample were microtomed into 5 mm thickness sections after dehydrating in a graded alcohol series and embedding in paraffin. H&E (Sigma-Aldrich, USA), alcian blue (AB, Sigma-Aldrich, USA) and Masson's trichrome (MT, Sigma-Aldrich, USA) staining were performed. The samples were analysed under a light microscope. Additionally, the tissue slides were stained with 4,6-diamidino-2-phenylindole (DAPI, Invitrogen, USA) to confirm the absence of cell nuclei in the DP.

2.3. DNA isolation and quantification of NP and DP

DNA was isolated from NP and DP using QIAamp DNA Mini Kit (Qiagen, USA) according to the manufacturer instructions. The total DNA content was quantified using DNA Quantitation Kit (Sigma-Aldrich, USA) as per the manufacturer instructions. Additionally,

the extracted DNA from NP and DP were electrophoresed on 1% agarose gel with DNA ladder.

2.4. Fabrication of placental derived extracellular matrix sponge (PEMS) from DP

The DP was rinsed with PBS thrice and homogenized using a blender [tissue/water mixture (2:1)] at room temperature for 15 min. The decellularized placental extracts were centrifuged at 8000 r.p.m for 20 min and the supernatant was discarded. The process was repeated several times to ensure that SDS does not remains in the decellularized placenta extracts. The final decellularized placental ECM and distilled water (2:1; v/v) mixed homogeneously, poured gently into moulds of required dimensions, frozen at – 80 °C, and freeze-dried for 72 h to get PEMS.

2.5. GAGs and collagen quantification of NP and PEMS

The GAGs content was assessed by quantifying the amount of sulphated glycosaminoglycans (sGAGs) content in NP and PEMS (n = 5). sGAGs was determined by modified alcian blue assay as reported elsewhere.[28] The sGAGs were extracted from NP and PEMS by digesting with 0.1 M phosphate buffer solution (pH 6.8) containing 10 mM cystein hydrochloride (Sigma-Aldrich, USA), 125 μg/mL papain (Sigma-Aldrich, USA) and 2 mM EDTA (Sigma-Aldrich, USA) at 60 °C for 60 h and supernatant was collected by centrifuging at 13,000 rpm for 20 min. The absorbance was measured at wavelength of 595 nm with iMark™ microplate reader. The standard curve was generated using chondroitin sulphate A (Sigma-Aldrich, USA) and used for estimating the sGAGs in samples.

The total collagen was quantified by hydroxyproline assay kit (Sigma-Aldrich, USA) according to the manufactures instruction. NP and PEMS (n = 5) were digested with 1% (w/v) pepsin (Sigma-Aldrich, USA) dissolved in 0.5 M acetic acid for 24 h at room

temperature to extract acid/pepsin soluble collagen. The digested suspension was centrifuged at 5000 r.p.m for 30 min at 4 °C and the supernatant was used for collagen quantification.

2.6. Scanning electron microscopy (SEM) and porosity measurement

For analysis of PEMS microstructure, PEMS were fixed with 4 % paraformaldehyde, dehydrated in graded ethanol series and gold coated for 30 s under high vacuum. The samples were observed using SEM (Carl Zeiss SMT AG, Germany).

The porosity is calculated as described elsewhere[29] by determining the volume (V) and mass (m) of the PEMS. Porosity of PEMS was calculated from the formula below:

$$\text{Porosity (\%)} \quad \left[1 - \frac{ds}{dp} \right] \text{ X } 100$$

where ds and dp are the density of the PEMS and average protein density (1.32 g/cm^3), respectively.

2.7. Swelling behaviour of PEMS

The swelling behaviour of PEMS was investigated at 37 °C in PBS (pH 7.4) for 64 h. The excess PBS in the PEMS was wiped gently with filter paper and weighed instantly on an electronic scale (Mettler-Toledo International Inc., USA). The content of PBS in the swollen PEMS was calculated as follows:

$$\text{Swelling ratio (\%)} = \frac{T_s - T_d}{T_s} \text{ x } 100$$

where T_s and T_d are the weights of the wet and dry PEMS, respectively. The experiments were run in triplicate and averaged.

2.8. Sodium dodecyl sulfate-polyacrylamide gel electrophoresis (SDS-PAGE) and western blotting of NP and PEMS

NP and PEMS were homogenized using a tissue homogeniser in a buffer containing protease inhibitor cocktail (Sigma-Aldrich, USA), 65 mM DTT, 4M guanidine HCl and 10 mM EDTA in 50 mM sodium acetate. The mixture was vortexed and subjected to ultrasonic homogenization on ice at 40% power and 50% pulse rate for a repeated 3 min cycles. The supernatant was collected after centrifuging the samples at 13,000 ×g for 30 min at 4 °C. Total protein concentration of the homogenates was measured by bicinchoninic acid assay kit (Thermo Scientific, Rockford, USA). 1D gel electrophoresis was executed with the extracted proteins from NP and PEMS. Protein resolved in 10% PAGE was fixed and stained with comassie blue staining.

For western blotting**,** 40 µg of protein was resolved in SDS-PAGE and electro-blotted onto nitrocellulose membrane (Millipore, USA) in Tris-Glycine buffer at 90V for 2 h. Membranes were incubated with a primary antibody [BMP-4 (Santa Cruz, USA), TGFβ1 (Abcam, USA), VEGF (Abcam, USA) and PLGF (Abcam, USA)] at 4 ºC overnight after blocking with 5% fat-free milk in PBST. The blots were washed with PBST and incubated for 1 h with secondary antibody (horseradish peroxidase conjugated). Pierce ECL-western blotting substrate was used to visualize the immunoreactive proteins as per manufacturer's instructions (Thermo Scientific, USA). Images were developed by automatic X-ray film processor and analysed using ImageJ (Rasband WS; NIH).

2.9. Compressive strength measurement and nanoindentation of PEMS

For compressive strength measurement, cylindrical PEMS in dry and wet state of cross-sectional area 122.7 mm^2 (diameter: 12.5 mm) were assessed by universal testing

machine (25K machine, Hounsfield, UK) at crosshead speed of 0.25 mm/min using 5000 N load cell. The wet samples were equilibrated with PBS for 1 h prior to compressive testing.

Nanoindentation of PEMS were carried out using nanoindenter (TI 950 TriboIndenter, Hysitron Inc., USA). A total number of 20 points at the distance of 5 μm was analysed for each sample by applying a maximum load of 25 μN with loading and unloading time period of 10s. Hardness and modulus were also obtained for the PEMS.

2.10. Yield strain and strain recovery measurements of PEMS

Yield strain and strain recovery measurements of PEMS were carried using a protocol as described in our previous publication.[30] Briefly, amplitude sweep was carried out on PEMS soaked in PBS overnight using a Bohlin CVO Rheometer (Malvern Instrument, UK) at a constant frequency of 1 Hz by shearing them until structure breakdown, to determine the yield strain. Also, at a frequency of 1 Hz with 0.01% applied strain for 150 s and 100% applied strain for 150 s, self-recovery analysis of PEMS were carried out. The above sequence segments was repeated twice to inspect the strain reversibility. For repeatability, ten samples were measured for PEMS.

2.11. Isolation of human amniotic mesenchymal stem cells (HAMSCs)

HAMSCs was isolated as described elsewhere[31] with modifications. According to the Institutional Ethical Committee approval, human placentas were obtained from subjects at Midnapore Medical College and Hospital after getting written informed consent. Briefly, term placentas obtained were transported to the laboratory under stringent sterile conditions, rinsed in HBSS media (Gibco, USA) containing 200 U/ml penicillin and 200 μg/ml streptomycin. Through a blunt dissection, amniotic membrane was separated from chorion and then subjected to two 30 minutes digestion with 0.05% trypsin-EDTA solution (Gibco, USA) and the supernatant was discarded. The tissue was washed with EBSS (Gibco, USA)

and underwent digestion with 10 U/ml DNase I (Sigma-Aldrich, USA) and 2 mg/ml Collagenase Type IV (Gibco, USA) for 60 min. After digestion, the cells pellet was collected by centrifugation. The cell pellet was suspended in DMEM low glucose medium (containing 10% FBS, streptomycin 100 µg/ml and penicillin 100 U/ml) and seeded in flasks (Nunc, USA) which is transferred to the incubator. The cells were passaged using 0.25% Trypsin-EDTA (Gibco, USA) and used for further experiments. The isolated cells were analysed for their immunophenotypical profile by flow cytometry/immunofluorescence and gene expression by RT-PCR as described in supporting information.

2.12. Cytotoxicity test/morphological assessment/apoptosis analysis

Cytotoxicity of PEMS was carried out by indirect cultivation of HAMSCs with PEMS conditioned media using a method as described elsewhere.[32] For preparation of PEMS conditioned medium, PEMS (diameter: 10 mm; height: 5mm) were incubated in 2 mL DMEM low glucose medium (containing 10% fetal bovine serum, 100 µg/ml streptomycin and 100 U/ml penicillin) for 72 h at 37 °C under sterile condition. 2.5 X 10^4 HAMSCs were seeded and cultivated in 24-well tissue culture plates for desired time periods either with PEMS conditioned or normal medium. Vybrant® MTT Cell Proliferation Assay Kit (Invitrogen, USA) was used to calculate the number of viable cells according to the manufactures instruction.

For morphological assessment, HAMSCs were cultured in lysine coated coverslips placed in 12 well plate either with PEMS conditioned or normal medium. The coverslips were removed at desired time of interest and stained with rhodamine (Invitrogen, USA) and DAPI (Invitrogen, USA) according to the manufacturer's protocol to analyse the cells.

Apoptosis of HAMSCs was investigated after exposing cells in PEMS conditioned media. Briefly 1.0 X 10^5 HAMSCs were seeded in 12 well tissue culture plates with lysine

coated coverslips and cultivated for 14 days either with normal medium or PEMS conditioned medium. After 14 days of cultivation, the cells were analysed for apoptosis using DeadEnd™ Fluorometric TUNEL System (Promega, USA) as per the manufacturer instruction.

2.13. Evaluation of HAMSCs integration into PEMS by live-dead staining/SEM

The PEMS was immersed in DMEM low glucose containing 10% fetal bovine serum, 100 µg/ml streptomycin and 100 U/ml penicillin for 24 h before cell seeding. Third passage HAMSCs were harvested and seeded onto the PEMS at a density of 1 x 10^6 cells/cm^2 in a 24-well plate. The culture medium was changed twice weekly. Cell viability on the PEMS was assessed using the live-dead cell staining kit (Invitrogen, USA) as per the manufacturer's instruction after 14 days of cultivation. Also, cell seeded PEMS were observed using SEM (Carl Zeiss SMT AG, Germany) to visualise the HAMSCs integration into PEMS after fixing in 4% paraformaldehyde.

2.14. HAMSCs culture on PEMS in chondrogenic or osteogenic induction media

The PEMS (diameter: 10 mm; height: 5 mm) was sterilized and incubated for six hours in cell culture medium prior to HAMSCs seeding. After removal of the excess medium from PEMS, each scaffold was seeded with one million cells. After 24 h, the culture medium was discarded and replaced either with osteogenic or chondrogenic medium. The osteogenic medium consists of 10% FBS, 100 µg/ml streptomycin and 100 U/ml penicillin, 10 mM β-glycerol-phosphate, 50 µM ascorbate-2-phosphate and 0.1 µM dexamethasone. The chondrogenic medium consists of 100 µg/ml streptomycin & 100 U/ml penicillin, 0.2 mM ascorbic acid-2-phosphate, 10^{-7} M dexamethasone, 10 µg/ml insulin, 5.5 µg/ml transferrin, 6.7 ng/ml selenium, 0.2 µg/ml ethanolamine (Gibco, USA), 10 ng/ml TGF-β3 (Gibco, USA) and 35 µM proline.

2.15. Immunohistological study for osteogenic/chondrogenic Differentiation of HAMSCs on PEMS

PEMS cultivated in osteogenic/chondrogenic medium for 21 days were fixed with 4% paraformaldehyde. PEMS was embedded in paraffin and sectioned using microtome. The tissue sections were permeabilized with 0.1 % Triton X-100 for 15 min and for reducing non-specific background, 1% bovine serum albumin was used. To analyse the differentiation of HAMSCs towards chondrogenic and osteogenic lineage, sections were stained with primary anti-COL II and anti-COL I (1:100; Abcam, USA) antibody, respectively. In both the cases Alexa Fluor® 488 Goat anti-rabbit secondary antibody (1:500; Invitrogen, USA) was used.

2.16. Gene expression of chondrogenic and osteogenic differentiation through reverse transcriptase–PCR (RT-PCR)

After culturing the HAMSCs seeded PEMS in osteogenic/chondrogenic medium for the desired time period of interest (1 and 21 days), the PEMS-HAMSCs construct (n = 5) were ground to a powder using liquid nitrogen. The resulting powder was immersed in TRIzol reagent (Invitrogen, USA) and RNA was extracted according to the manufacturer's instructions. cDNA was synthesised from the isolated RNA using cDNA synthesis kit (Thermo Scientific, USA) according to the manufacturer's protocol. PCR amplification with the gene specific primers (supporting information Table S1.) was performed in a thermal cyclers (Eppendorf Mastercycler, USA) and the PCR product imaged in UV gel doc (Bio-Rad, USA) after running it in 1% agarose gels. The band intensity was analysed using ImageJ (Rasband WS; NIH)

2.17. Evaluation of the host response to implanted PEMS *in vivo*

In vivo studies were performed according to the animal ethical committee guidelines (Indian Institute of Technology Kharagpur). To evaluate the host response of the PEMS *in*

vivo, subcutaneous implantation was performed in New Zealand white rabbits (2.5–3 kg; n = 3 per group). Before transplantation of the PEMS, an injection of ketamine hydrochloride was used to anesthetize the rabbits. Transverse incision was made and subcutaneous implantation of PEMS was performed. Free access to food and water was provided to the rabbits after surgery. After 28 days post-transplantation, rabbits were sacrificed and PEMS retrieved with surrounding tissues were fixed in 10% paraformaldehyde and processed for H&E, TB and MT staining.

2.18. Animal model for osteochondral defect

New Zealand white rabbits (2.5–3 kg) maintained in stainless-steel cages with adequate diet supplements. Rabbits were anaesthetized with ketamine hydrochloride followed by creation of three osteochondral cylindrical defects (4 mm in diameter and 5 mm deep) with a sterilized stainless-steel drill bit. Out of 3 cylindrical defects in an animal, one was left untreated (Empty Defect), one implanted with the cell-free PEMS (CFP) and one with cell-seeded PEMS (CSP) (n = 5). For CSP, HAMSCS were cultivated in PEMS for 7 days prior to implantation in the defect site. Rabbits were sacrificed 60 days post-implantation and specimens retrieved with surrounding tissues for inspection. The specimens were also fixed, decalcified, dehydrated in an ethanol series, and embedded in paraffin. Consecutive sections of 3 μm thicknesses were microtomed and stained with toluidine blue (TB) for the detection of cartilage deposition, cellularity and to understand the healing process. Further, sections were immunostained for COL I/II (Abcam, USA) according to the manufacturer's instructions. According to the ICRS visual histological assessment grading scale (supporting information Table S2) semi-quantitative histomorphological analysis was performed and a representative score for each parameter was determined by averaging the scores of three blinded observers.

2.19. Statistical analysis

For statistical investigation and interpretation of significant differences between experimental groups, one-way ANOVA student's two-tailed t-test was performed using GraphPad Prism software (version 5.02, La Jolla, CA, USA). The level of significance was determined as $p < 0.05$. All data were represented as mean ± standard deviation (SD).

3. RESULTS

3.1. Decellularization of human placenta and its histological analysis

In the present study, decellularization of placenta was achieved by a combinatorial treatment of SDS and nucleases. After the decellularization process, the placenta turned to milky white in colour which represented cell removal. The effectiveness in removal of the cellular components was assessed by H&E and DAPI staining. H&E staining revealed complete absence of cells and nucleic acids in DP indicating successful decellularization and in case of NP, abundant cellular components were present (Fig. 1A and B). Major ECM components such as GAG and collagen of NP and DP were assessed by AB and MT staining, respectively. It is observed that GAG (Fig. 1C and D) and collagen (Fig. 1E and F) were retained in DP after decellularization process. Further, the presence and absence of DNA in NP and DP, respectively, was confirmed by DAPI staining (Fig. 1G and H). The DNA from both NP and DP were isolated and quantified. From Fig. 2A, it is observed that the DNA content of DP (35.2 ± 11.2 ng/mg tissue) was significantly reduced by the decellularization process compared to NP (1235.2 ± 224.5 ng/mg tissue). Extracted DNA sample from DP did not reveal any DNA fragments on the 1% agarose gel (Fig. 2B) which is in accordance with the results of H&E/DAPI.

3.2. Fabrication of PEMS and its physico-chemical characterization

NP (Fig. 3A) was successfully fabricated into PEMS (Fig. 3B) through decellularization, molding and lyophilization process. The SEM micrographs of PEMS revealed microstructure with high degree of porosity and interconnectivity (Fig. 3C). The porosity is considered to be an important criterion since it is necessary for nutrient/gas transport and cell infiltration. The porosity of PEMS was found to be 93.5 ± 2.9.

To evaluate the biochemical preservation after PEMS fabrication, PEMS was quantified for major ECM components such as collagen and GAG. As shown in Fig. 3D, PEMS after decellularization treatment retained collagen (403.6 ± 44.1 μg/mg) and GAG (41.7 ± 10 μg/mg) which is not significantly different ($P > 0.05$) to the collagen (454.2 ± 21.9 μg/mg) and GAG (52.9 ± 4.8 μg/mg) content of NP. These results demonstrated that after decellularization process the major ECM components was effectively retained.

The swelling behaviour and structural stability of PEMS influences not only the maintenance of scaffolds shape but also are critical in mediating the rate of nutrition and waste transport within the scaffolds. Swelling kinetics of PEMS was shown in Fig. 3E. PEMS when exposed to PBS for 0.5 h demonstrated ~ 75% swelling associated with rapid water-uptake. After which, it attained a plateau and no further increase in mass was observed till 64 h. Long-term swelling study is essential for more critical assessment.

3.3. SDS PAGE and western blotting of NP and PEMS

To investigate the proteins retained after the decellurization process, the solubilized PEMS and NP were assessed by SDS-PAGE. Fig. 4A revealed the presence of various proteins/peptides in the PEMS which demonstrated the complexity of the PEMS. Also the presence of several proteins and peptides in the PEMS will be beneficial to the HAMSCs in

promoting their cellular activities. These results are in accordance with the previous studies.[33,34]

Western blotting was performed to detect the presence of endogenous bioactive molecules (BMP-4, TGFβ1, VEGF and PLGF) which was known to regulate the bone, cartilage and blood vessel regeneration. Fig. 4B revealed that, PEMS retained BMP-4, TGFβ1, VEGF and PLGF after the decellurization process. Although, there has been reduction in the amount of bioactive molecules in PEMS compared with the NP, there was no significant difference ($p > 0.05$) observed in the relative band intensity (Fig. 4C).

3.4. Compressive strength measurement and nanoindentation of PEMS

The compressive modulus of PEMS in dry and wet conditions was found to be 289.8 ± 7.6 kPa and 173.5 ± 4.9 kPa, respectively. Similarly, the compressive strength of PEMS in dry and wet conditions was found to be 75.0 ± 1.5 kPa and 36.2 ± 2.1 kPa. It is observed that the compressive properties of PEMS was decreased significantly in wet condition due to its significant swelling.

The viscoelastic property of PEMS was demonstrated by nanoindentation study as shown in Fig. 5A. . PEMs displayed significant elastic like response with displacement up to 800 nm under 25 μN load. Thus, it displays self-recovery of 600 nm with removal of external load with permanent deformation of ~200 nm. The hardness (H) and modulus values (E_r) for PEMS were 2.66 ± 0.52 MPa and 12.28 ± 0.84 MPa, respectively.

3.5. Yield strain and strain recovery measurements of PEMS

Strain amplitude sweeps of PEMS (Fig. 5B) demonstrated an elastic response indicating PEMS represented a characteristic behaviour of hydrogels under wet condition. At 0.001 strain, the G' and G" values of PEMS were 1731 Pa and 188.83 Pa, respectively. Above

the critical strain (0.084%), storage modulus of the PEMS decreased rapidly due to breakdown of the network structure.

From Fig. 5B, the G′ response which is characterized by the linear stress-strain curve, was attained until 0.084% applied strain, beyond which the PEMS network structure started to yield. Accordingly, strain reversibility study of PEMS was carried out at 0.01% strain (within the linear viscoelastic region) for degree of elasticity and at 100% strain for breakdown of the network followed by measurement at 0.01% strain to assess the degree of network recovery. Interestingly from Fig. 5C at large-amplitude oscillatory strain (100%), the network structure of PEMS was almost disrupted and the magnitude of complex modulus was declined from ~ 12 kPa to 750 Pa. On the other hand, when the amplitude strain was reduced to 0.01%, PEMS almost regained its initial structure, leading to the retrieval of the complex modulus close to its initial value representing self-recovery.

3.6. Cytotoxicity test/morphological assessment/apoptosis analysis

The MTT cytotoxicity assay was performed to test remnant toxic chemical residues that may be present in the PEMS as a result of decellularization. As observed from Fig. 6A, there was an increased cellular metabolic activity of HAMSCs cultured in the PEMS conditioned medium compared to the HAMSCs cultured in normal medium, demonstrating the absence of cytotoxic effects of the PEMS conditioned medium. After 14 days, it is evident that HAMSCs proliferated at a higher rate when it is cultured in PEMS conditioned medium (2.88×10^5) compared to the normal medium (2.48×10^5). This may be due to the presence of PEMS bioactive molecules in the conditioned media.

From Fig. 6B, it can be clearly visualised that HAMSCs cultured in PEMS conditioned medium provided a favourable environment for HAMSCs and cells proliferated rapidly. After 96 h, the HAMSCs cultured in PEMS conditioned medium displayed well

spread cytoskeleton which is similar to HAMSCs cultured in normal medium. Further, the HAMSCs were able to contact each other with the cellular protrusions and extensions. There is no difference in the morphology of HAMSCs cultured in PEMS conditioned medium compared with the normal medium.

After 14 days of HAMSCs cultivation either in normal and PEMS conditioned medium, tunnel assay was performed to detect apoptosis. As it can be seen from Fig. 7A and B, PEMS conditioned medium did not cause deleterious effect and there was no difference in the number of apoptotic cells, on the cells cultured in PEMS conditioned medium compared with the normal medium, indicating that PEMS conditioned medium does not trigger apoptosis.

3.7. Evaluation of HAMSCs integration into PEMS by live-dead Staining/SEM

Adhesion and viability of HAMSCs within PEMS were evaluated by live-dead cell staining (Fig. 8A). After 14 days, it was observed that PEMS supported the HAMSCs attachment, infiltration and proliferation since PEMS have abundant bioactive residues. Fig. 8A revealed that there were no dead cells (red) in PEMS and dense formation of live cell (green) sheet on the PEMS was visualized which demonstrated that PEMS is a promising biocompatible scaffold for HAMSCs. According to SEM after 14 days of cultivation (Fig. 8B), large number of well spread HAMSCs sheets were found throughout PEMS, which supports the inference of live-dead staining.

3.8. Immunohistological study for osteogenic/chondrogenic differentiation of HAMSCs on PEMS

The supportive role of PEMS in differentiation of HAMSCs into the osteogenic/chondrogenic lineage was evaluated through immunohistochemical imaging. Immunohistochemical staining revealed that the osteogenic-induced HAMSCs secreted COL

I within the PEMS, after 21 days of culture time (Fig. 9A). Also, Fig. 9B indicated that chondrogenic-induced HAMSCs secreted COL II within the PEMS, after 21 days of culture time. In both the cases, it was observed that COL I/II were uniformly distributed throughout the entire PEMS. These results demonstrates that PEMS can support both osteogenic and chondrogenic differentiation of HAMSCs by induction.

3.9. Gene expression for chondrogenic and osteogenic differentiation by RT - PCR

The expression of chondrogenic-related genes (COL II, ACAN and SOX9) and osteogenic-related genes (COL I, OPN and OCN) were evaluated. From Fig. 9C and D, it is observed that genes coding for COL II, ACAN and SOX9 were all upregulated at day 21 compared to day 1, which states that the chondrogenic-induced HAMSCs could differentiate toward chondrocytes within the PEMS. Similarly, expression levels of osteogenic-related genes (COL I, OPN and OCN) were all upregulated at 21 days indicating the osteogenic differentiation potential of HAMSCs within PEMS (Fig. 9C and D). The housekeeping gene GAPDH on day 1 and 21 was expressed at similar levels.

3.10. Evaluation of the host response to implanted PEMS *in vivo*

To evaluate and understand PEMS immune response and integration into the host tissue, PEMS were implanted subcutaneously in the back of rabbits and were retrieved after 28 days. The PEMS subcutaneously implanted rabbits appeared consistently healthy and no deaths were recorded throughout the study period. After 28 days of PEMS implantation, PEMS were retrieved with surrounding tissues and histologically analysed. According to H&E staining (Fig. 10A) no adverse chronic inflammatory responses were found and large number of blood vessels (neo-capillary formation) were found throughout PEMS. This demonstrated the ability of PEMS to attract blood vessels. The interface layer had many oriented fibroblasts and no giant cells were observed. Also, significant tissue *in-growth*/close

integration of the implanted PEMS and host tissue was also observed. TB staining (Fig. 10B) revealed small number of mast cells in surrounding tissue around the PEMS and also few mast cells were found infiltrated to the PEMS. This mild inflammatory response after PEMS implantation is attributed to the earlier inflammatory response phase which is similar to normal wound healing process. From MT staining (Fig. 10C) new dense collagen deposition was visualised around the PEMS demonstrating stimulated cell infiltration. No capsular layer/fibrosis was found around the surrounding tissue of PEMS.

3.11. Animal model for osteochondral defect

The maintenance of appropriate mechanical properties, and cytocompatibility are critical elements for scaffold design in tissue engineering. PEMS with its ability to support HAMSC proliferation/differentiation along with its favourable viscoelastic and strain reversibility properties were examined for its ability to accelerate the healing process in osteochondral defects. All of the experimental rabbits survived surgery and there were no postoperative complications. Fig. 10D shows the representative optical image of the created defects. The defects sites were filled with cell-seeded PEMS (CSP), cell-free PEMS (CFP) and empty defect (ED) as shown in Fig. 10E. The animals were sacrificed after 60 days and complete joints were collected for gross observation and histological analysis. In case of defects treated with cell-seeded PEMS (CSP), it can be macroscopically observed from Fig. 10F that the defects were filled with white shiny repair tissue and there was no distinguished border between the neo-cartilage and the surrounding normal tissue demonstrating uniform/good integration with the newly formed tissues. On the other hand, the defects treated CFP and ED had a distinct boundary between the newly formed tissue and the existing tissue and were covered with a brownish mass.

On further examination with TB staining after 60 days of implantation, it was seen that the CSP and CFP has not completely degraded in the defect site (marked with stars) signifying that viscoelastic and strain reversibility support was provided throughout the 60 day period. In case of ED (Fig. 11A1 and 11A5), the defects were filled with minimal reparative tissue with irregular distribution of the trabecular bone. Also chondrocyte matrix were visible only at the junction of the native tissue (Fig. 11A2 and 11A6); at the defect sites, empty spaces were observed between the neo-tissues formed (Fig. 11A3 and 11A7). Moreover, mechanically instable fibrous tissues (fibroblast-like cells) were present in empty defects with minimum proteoglycan deposition signifying improper healing (Fig. 11A4 and 11A8).

Quite the reverse, the CFP were almost fully filled with repaired tissue and good integration of the PEMS with surrounding reparative tissue was observed. However, some instable fibrous tissues were also observed in CFP (Fig. 11B1 and 11B5). Neo-bone tissue formed around the porous scaffold in CFP (Fig. 11B6). Also, increase in the osteoblast-like cells lining the trabecular bone was present in defects filled with CFP compared to ED (Fig. 11B3, 11B4, 11B7 and 11B8). At 60 days after transplantation, defects filled will CSP were greatly infiltrated with repaired tissue. The regenerated cartilage tissue showed good integration with the newly formed subchondral bone (Fig. 11C1, 11C2, 11C5 and 11C6). The bone regeneration was not complete due to the incomplete degradation of CSP (Fig. 11C3 and 11C7). In some areas, fibrous layer with cluster of chondrocytes were found in addition to new bone formation (Fig. 11C4 and 11C8).

Immunohistochemistry results demonstrated immunopositivity for COL I to varying extents for defects treated with ED, CFP and CSP, respectively, after 60 days of implantation (Fig. 12A-C). It is observed that COL I expression was evidently more in area and intense for defects filled with CSP (Fig. 12C) compared to defects treated with CFP (Fig. 12B) and ED

(Fig. 12A). Also, COL I was mostly detected in the peripheral zone of the subchondral bone. Numerous osteoblasts are seen lining the subchondral bone in CSP and CFP indicating the area of remodelling and therefore presence of COL I is reasonable in the peripheral region. In sharp contrast, COL I was detected with very less intensity in case of ED.

COL II staining in ED, CFP and CSP were shown in Fig. 12D-F. Cartilage tissue consisting of chondrocytes within the lacunae was present in all types of defects - ED, CFP and CSP. However, the radial orientation of cartilage was missing in ED as well as CFP (Fig. 12D and E). The chondrocytes in ED mostly appeared as individual cells with irregular organisation, whereas some chondrocytes in the deeper zone of defects implanted with CFP were organised in clusters and aligned perpendicular to the articular surface. On the other hand, CSP demonstrated matured cartilage with superficial layer, radial orientation of chondrocytes and calcified cartilage overlying the subchondral bone demonstrating mechanically stable tissue with load bearing abilities (Fig. 12F).

From the histomorphometric analysis it is evident that the defects filled with CSP is found to support superior osteochondral regeneration compared to CFP and ED after 60 days of implantation. Also from the histological grading scores (Table 1.), the CSP scored significantly higher than the CFP ($p < 0.05$) and the control group ($p < 0.05$).

Table 1. Histological Scores for Samples Retrieved after 60 days

Score Parameter	Empty Defect (ED)	Cell-Free PEMS (CFP)	Cell-Seeded PEMS (CSP)
Surface	0.3 ± 0.14	0.5 ± 0.03	1.6 ± 0.61
Matrix	0.3 ± 0.11	1.3 ± 0.31	2.6 ± 0.21
Cell distribution	0.3 ± 0.15	1 ± 0.12	2.6 ± 0.16
Cell population viability	0.6 ± 0.11	1.3 ± 0.18	1.6 ± 0.58

Subchondral bone	1 ± 0.06	1.3 ± 0.43	1.6 ± 0.51
Cartilage mineralization	0.6 ± 0.09	0.9 ± 0.05	1.7 ± 0.75
Total	3.1 ± 0.66	6.3 ± 1.12	11.7 ± 2.82

For each parameter, values are expressed as mean ± SD. Total score of CFP significantly higher ($p < 0.05$) than ED; Total score of CSP significantly higher ($p < 0.05$) than ED; Total score of CSP significantly higher ($p < 0.05$) than CFP;

4. DISCUSSION

To promote accelerated regeneration of osteochondral injuries, it is essential to have a bioactive scaffold that can deliver the required physical, mechanical and biochemical factors. In this context, human placenta which are commonly discarded bio-waste can be harvested without harm to the donor and effectively used to fabricate porous scaffold by the decellularization process. Also, the extracellular matrix components and bioactive molecules can be retained within the scaffold to maintain the bioactivity which will support HAMSCs in proliferation and differentiation towards the bone & cartilage.

In the present study, we used decellularization protocol (SDS, trypsin, RNase and DNase) to fabricate biomimetic placental derived extracellular matrix sponges (PEMS) for accelerated osteochondral tissue regeneration. We used SDS and trypsin in mild concentrations to solubilize the cell membrane without degrading the extracellular matrix components. Additionally, DNase and RNase were used to remove fragmented DNA/RNA completely to minimalize any adverse immune response. The fabricated PEMS resulted in complete removal of cellular contents which is evidenced by (a) absence of detectable nuclear material in the tissue sections stained with H&E and DAPI; (b) DNA quantity less than 50 ng/mg; and (c) no visible DNA bands in agarose gel. Also, the major ECM

components (collagen and GAGs) which play the crucial role in proliferation, migration and differentiation of cells were thoroughly preserved. From western blot analysis, it is observed that bioactive molecules (BMP-4, TGFβ1, VEGF and PLGF) that are known for bone, cartilage and blood vessel development/regeneration were retained within the PEMS.

The mechanical property of the scaffolds is considered to be a critical aspect when addressing cartilage tissue regeneration. In this context, the wet compressive modulus of the PEMS was much higher than the protein based porous scaffolds reported for cartilage tissue engineering in the literatures.[32,35] But mechanistically the compressive modulus of PEMS was significantly lower than the human articular cartilage (ranging from 1.9 to 14.4 MPa).[36,37] Also, PEMS with its ability to withstand alternate strain and relaxation could be beneficial for treating osteochondral tissue defects, where high strain and cyclic loading is experienced.[30]

The SEM images of PEMS revealed interconnected fibrous architecture which along with its ~ 93% porosity and high swelling ratio will facilitate cell penetration deep into the scaffold. The cytotoxicity of PEMS was tested by indirect cultivation of HAMSCs with PEMS conditioned medium, since during the decellularization process of PEMS with SDS/trypsin many residual cellular components/SDS may have been retained in the PEMS which might be harmful for the cells. MTT and tunnel assay revealed that the PEMS conditioned media did not affect the HAMSCs metabolic activity and does not triggered apoptosis. Rhodamine & DAPI staining of HAMSCs grown in PEMS conditioned media did not show any morphological alterations compared to the HAMSCs grown in normal medium. Also, live dead staining and SEM images of HAMSCs-PEMS construct confirmed that HAMSCs successfully integrated and infiltrated into PEMS. Thus PEMS supported the adhesion, proliferation and infiltration of HAMSCs and hence proved to be non-cytotoxic *in vitro*. To investigate the potential of HAMSCs to differentiate towards chondrogenic and osteogenic lineage *in vitro,* we used immunohistochemical staining and RT-PCR analysis.

HAMSCs seeded on PEMS cultivated in chondrogenic induction media for 21 days demonstrated secretion of COL II and the expression of chondrogenic genes (COL II, ACAN and SOX9) were upregulated. Similarly, HAMSCs seeded on PEMS cultivated in osteogenic induction media for 21 days demonstrated secretion of COL I and the expression of osteogenic genes (COL I, OPN and OCN) were upregulated. Taken together, these findings strongly suggests that PEMS supports both chondrogenic and osteogenic differentiation of HAMSCs.

It is essential to evaluate the immune reaction *in vivo* before transplantation to analyse the healing ability of PEMS in osteochondral defect model. In this context, subcutaneous implantation of PEMS is considered to be the first phase for the assessment of the *in vivo* biocompatibility. Histological analysis of the subcutaneous implanted PEMS after 28 days revealed no severe graft rejection (absence of tissue necrosis or granulomatous inflammation) with no fibrous layer formation surrounding the PEMS was observed. Also, PEMS further demonstrated its outstanding biocompatibility *in vivo* by supporting blood vessel formation. Overall, the absence of any adverse immune reaction in the host animals demonstrated that the implanted PEMS were biocompatible *in vivo*.

Xenotransplantation of mesenchymal stem cells for osteochondral tissue defects is advantageous since it might help to reduce donor site morbidity associated with autotransplantation, its relative abundant supply and ease of use. There are very few literatures about the xenotransplantation of mesenchymal stem cells for osteochondral defect repair.[38,39] In this context due to the non-availability of non-autologous human model for ethical reasons, we used xenogeneic transplantation of human mesenchymal stem cells in an animal model to investigate the possibility of xenotransplantation of mesenchymal stem cells. In order to evaluate the potential of PEMS in accelerating the healing of osteochondral defects, CFP and CSP were implanted in the osteochondral defects in the rabbit model and

were compared with ED. Histological scores for samples retrieved after 60 days revealed that xenotransplantation of HAMSCs using PEMS (CSP) effectively repaired osteochondral defect in a rabbit model compared to CFP and ED. Also, CFP is found to facilitate better healing compared with ED. The possible reasons for CSP and CFP for promoting efficient osteochondral repair compared to ED might be due to (a) PEMS ability to withstand alternate strain and relaxation; (b) the bioactive molecular cues retained in the PEMS might have contributed in the healing of osteochondral defect; (c) the immunosuppressive potential of HAMSCs which might have helped in preventing graft rejection and might have promoted good integration with the host environment promoting better healing of the defect.

However, this study could be extended for clinical applications after addressing several critical issues such as (a) in depth protein profiling and validating the minimum critical density factor of bioactive cues present in the PEMS for tissue specific cellular activities; (b) understanding the *in vivo* release kinetic profile of the retained bioactive cues in PEMS; (c) evaluation of subcutaneous host response to the PEMS for longer time duration to understand the constructive tissue remodelling and (d) validating significant efficacy of PEMS in mediating osteochondral repair with large animal models. In addition, detailed understanding and investigation on xenotransplantation of mesenchymal stem cells constructs in treating osteochondral tissue defects are necessary to validate the results obtained in this study.

5. CONCLUSIONS

We successfully developed a biomimetic human placenta derived extracellular matrix sponges by decellurization process for osteochondral tissue engineering. The fabricated PEMS retained the natural extracellular matrix composition and the bioactive molecules known for bone, cartilage and blood vessel development/regeneration. Also, the PEMS

supported the viability, proliferation and differentiation of HAMSCs into chondrogenic/osteogenic *in vitro* upon induction. In addition, no immune rejection after subcutaneous implantation was observed. We also proved the ability of CFP and CSP to mediate early osteochondral repair in rabbit model. Therefore, this study provides an approach, where biological waste (human placenta) is converted into bioactive scaffold that has potential for osteochondral tissue engineering. Conceptually, to specifically match the individual requirements (e.g. mechanical properties, pore size) of bone and cartilage tissue, a composite biphasic PEMS will be evaluated by the authors in the future work.

DISCLOSURES

No conflicts of interest exist.

ACKNOWLEDGMENTS

Fellowship from Council of Scientific and Industrial Research (CSIR), Govt. of India, New Delhi is acknowledged for Arun Prabhu Rameshbabu and Paulomi Ghosh. Fellowship from Department of Science and Technology (DST) is acknowledged for Kamakshi Bankoti. Financial aid from DST, Defence Research & Development Organisation (DRDO), and CSIR, Govt. of India, New Delhi is acknowledged.

REFERENCES

1. Y. Wu, S. Zhu, C. Wu, P. Lu, C. Hu, S. Xiong and J. Chang, *et al.*, A bi-lineage conducive scaffold for osteochondral defect regeneration, *Adv. Funct. Mater.*, 2014, **24**, 4473–4483.

2. W. Wang, L. Sun, P. Zhang, J. Song and W. Liu, An anti-inflammatory cell-free collagen/resveratrol scaffold for repairing osteochondral defects in rabbits, *Acta Biomater.*, 2014, **10**, 4983–4995.

3. P. J. Emans, L. W. van Rhijn, T. J. Welting, A. Cremers, N. Wijnands and F. Spaapen, *et al*., Autologous engineering of cartilage, *Proc Natl Acad Sci.,* 2010, **107**, 3418–3423.

4. N. B. Kock, G. Hannink, A. van Kampen, N. Verdonschot, J. L. van Susante and P. Buma, Evaluation of subsidence, chondrocyte survival and graft incorporation following autologous osteochondral transplantation, *Knee Surg*. *Sports Traumatol. Arthosc.,* 2011, **19**, 1962–1970.

5. C. Chung and J. A. Burdick, Engineering cartilage tissue, *Adv. Drug Deliv. Rev*., 2008, **60**, 243–262.

6. L. P. Yan, J. M. Oliveira, A. L. Oliveira and R. L. Reis, Current concepts and challenges in osteochondral tissue engineering and regenerative medicine, *ACS Biomater. Sci. Eng.,* 2015, **1**, 183–200.

7. C. A. Vilela, C. Correia, J. M. Oliveira, R. A. Sousa, J. Espregueira-Mendes and R.L. Reis, Cartilage repair using hydrogels: a critical review of *in vivo* experimental designs, *ACS Biomater. Sci. Eng.,* 2015, **1**, 726–739.

8. C. W. Cheng, L. D. Solorio and E. Alsberg, Decellularized tissue and cell-derived extracellular matrices as scaffolds for orthopaedic tissue engineering, *Biotechnol. Adv.,* 2014, **32**, 462–484.

9. J. S. Choi, J. D. Kim, H.S. Yoon and Y. W. Cho, Full-thickness skin wound healing using human placenta-derived extracellular matrix containing bioactive molecules, *Tissue Eng. Part A,* 2013, **19**, 329–339.

10. M. T. Wolf, K. A. Daly, E. P. Brennan-Pierce, S. A. Johnson, C. A. Carruthers and A. D'Amore, *et al*., A hydrogel derived from decellularized dermal extracellular matrix, *Biomaterials,* 2012, **29**, 7028–7038.

11. S. Ponce Márquez, V. S. Martínez, W. McIntosh Ambrose, J. Wang, N. G. Gantxegui, O. Schein and J. Elisseeff, Decellularization of bovine corneas for tissue engineering applications, *Acta Biomater*., 2009, **5**, 1839–1847.

12. B. Weber, P. E. Dijkman, J. Scherman, B. Sanders, M. Y. Emmert and J. Grünenfelder, *et al*., Off-the-shelf human decellularized tissue-engineered heart valves in a non-human primate model, *Biomaterials,* 2013, **34**, 7269–7280.

13. S. Baiguera, C. D. Gaudio, E. Kuevda, A. Gonfiotti, A. Bianco and P. Macchiarini, Dynamic decellularization and cross-linking of rat tracheal matrix, *Biomaterials,* 2014, **35**, 6344–6350.

14. J. M. Fishman, M. W. Lowdell, L. Urbani, T. Ansari, A. J. Burns and M. Turmaine, *et al*., Immunomodulatory effect of a decellularized skeletal muscle scaffold in a discordant xenotransplantation model, *Proc. Natl. Acad. Sci*., 2013, **110**, 14360–14365.

15. L. K. Chan, V. Y. Leung, V. Tam, W.W. Lu, K.Y. Sze and K.M. Cheung, Decellularized bovine intervertebral disc as a natural scaffold for xenogenic cell studies, *Acta Biomater.,* 2013, **9**, 5262–5272.

16. G. Mazza, K. Rombouts, A. R. Hall, L. Urbani, T. V. Luong and W. Al-Akkad, *et al*., Decellularized human liver as a natural 3D-scaffold for liver bioengineering and transplantation, *Sci. Rep.*, 2015, **5**, 13079.

17. F. Consolo, S. Brizzola, G. Tremolada, V. Grieco, F. Riva and F. Acocella, *et al*., A dynamic distention protocol for whole-organ bladder decellularization: histological and biomechanical characterization of the acellular matrix, *J. Tissue Eng. Regen. Med*., 2013, **4**, 1767–1778.

18. L. Wang, J. A. Johnson, Q. Zhang and E. K. Beahm, Combining decellularized human adipose tissue extracellular matrix and adipose-derived stem cells for adipose tissue engineering, *Acta Biomater.*, 2013, **9**, 8921–8931.

19. C. Quint, Y. Kondo, R. J. Manson, J. H. Lawson, A. Dardik and L. E. Niklason, Decellularized tissue-engineered blood vessel as an arterial conduit, *Proc. Natl. Acad. Sci.,* 2011, **108**, 9214–9219.

20. J. D. O'Neill, R. Anfang, A. Anandappa, J. Costa, J. Javidfar and H. M. Wobma, *et al*., Decellularization of human and porcine lung tissues for pulmonary tissue engineering, *Ann. Thorac. Surg*., 2013, **96**, 1046–1055.

21. O. Syed, N. J. Walters, R. M. Day, H. W. Kim and J. C. Knowles, Evaluation of decellularization protocols for production of tubular small intestine submucosa scaffolds for use in oesophageal tissue engineering, *Acta Biomater.*, 2014, **10**, 5043–5054.

22. M. J. Sawkins, W. Bowen, P. Dhadda, H. Markides, L. E. Sidney and A. J. Taylor, *et al*., Hydrogels derived from demineralized and decellularized bone extracellular matrix, *Acta Biomater*., 2013, **9**, 7865–7873.

23. K. Chen, X. Lin, Q. Zhang, J. Ni, J. Li and J. Xiao, *et al*., Decellularized periosteum as a potential biologic scaffold for bone tissue engineering, *Acta Biomater.,* 2015, **19**, 46–55.

24. R. Burgkart, A. Tron, P. Prodinger, M. Culmes, J. Tuebel and M. van Griensven, *et al*., Decellularized kidney matrix for perfused bone engineering, *Tissue Eng. Part C Methods*, 2014, **20**, 553–561.

25. M.C. Moore, V. Pandolfi and P. S. McFetridge, Novel human-derived extracellular matrix induces *in vitro* and *in vivo* vascularization and inhibits fibrosis, *Biomaterials*, 2015, **49**, 37–46.

26. K. E. Benders, P. R. van Weeren, S. F. Badylak, D. B. Saris, W. J. Dhert and J. Malda, Extracellular matrix scaffolds for cartilage and bone regeneration, *Trends Biotechnol.,* 2013, **31**, 169–176.

27. L. Flynn, J. L. Semple and K. A. Woodhouse, Decellularized placental matrices for adipose tissue engineering, *J. Biomed. Mater. Res. A*, 2006, **79**, 359–369.

28. S. B. Frazier, K. A. Roodhouse, D. E. Hourcade and L. Zhang, The quantification of glycosaminoglycans: a comparison of HPLC, carbazole, and alcian blue methods, *Open Glycosci.,* 2008, **1**, 31–39.

29. H. Fischer, I. Polikarpov and A.F. Craievich, Average protein density is a molecular weight dependent function, *Protein Sci.,* 2004, **13**, 2825–2828.

30. P. Ghosh, A. P. Rameshbabu and S. Dhara, Citrate cross-linked gels with strain reversibility and viscoelastic behavior accelerate healing of osteochondral defects in a rabbit model, *Langmuir,* 2014, **30**, 8442–8451.

31. F. Alviano, V. Fossati, C. Marchionni, M. Arpinati, L. Bonsi and M. Franchina, *et al*., Term amniotic membrane is a high throughput source for multipotent mesenchymal stem cells with the ability to differentiate into endothelial cells in vitro, *BMC Dev. Biol.,* 2007, **21**, 7:11.

32. B. Hoyer, A. Bernhardt, A. Lode, S. Heinemann, J. Sewing and M. Klinger, *et al*., Jellyfish collagen scaffolds for cartilage tissue engineering, *Acta Biomater.,* 2014, **10**, 883–892.

33. N. V. Welham, Z. Chang, L. M. Smith and B. L. Frey, Proteomic analysis of a decellularized human vocal fold mucosa scaffold using 2D electrophoresis and high-resolution mass spectrometry, *Biomaterials,* 2013, **34**, 669–676.

34. F. Pati, J. Jang, D. H. Ha, S. Kim Wom, J.W. Rhie and J.H. Shim, *et al.,* Printing three-dimensional tissue analogues with decellularized extracellular matrix bioink, *Nat. Commun.,* 2014, **5**, 3935.

35. Q. Zhang, H. Lu, N. Kawazoe, G. Chen, Pore size effect of collagen scaffolds on cartilage regeneration, *Acta Biomater.,* 2014, **10**, 2005–2013.

36. G. Zheng-Qiu, X. Jiu-Mei, Z. Xiang-Hong, The development of artificial articular cartilage—PVA hydrogel, Biomed. Mater. Eng. 1998, **8**:75–81.

37. R.A. Magnussen, F. Guilak, T.P. Vail, Cartilage degeneration in post-collapse cases of osteonecrosis of the human femoral head: altered mechanical properties in tension, compression, and shear, J. Orthop. Res. 2005, **23**, 576.

38. C. T. Laurencin and S. F. El-Amin, Xenotransplantation in orthopaedic surgery, *J. Am. Acad. Orthop. Surg.,* 2008, **16**, 4–8.

39. K. M. Jang, J. H. Lee, C. M. Park, H. R. Song and J. H. Wang, Xenotransplantation of human mesenchymal stem cells for repair of osteochondral defects in rabbits using osteochondral biphasic composite constructs, *Knee Surg. Sports Traumatol. Arthrosc.,* 2014, **22**, 1434–1444.

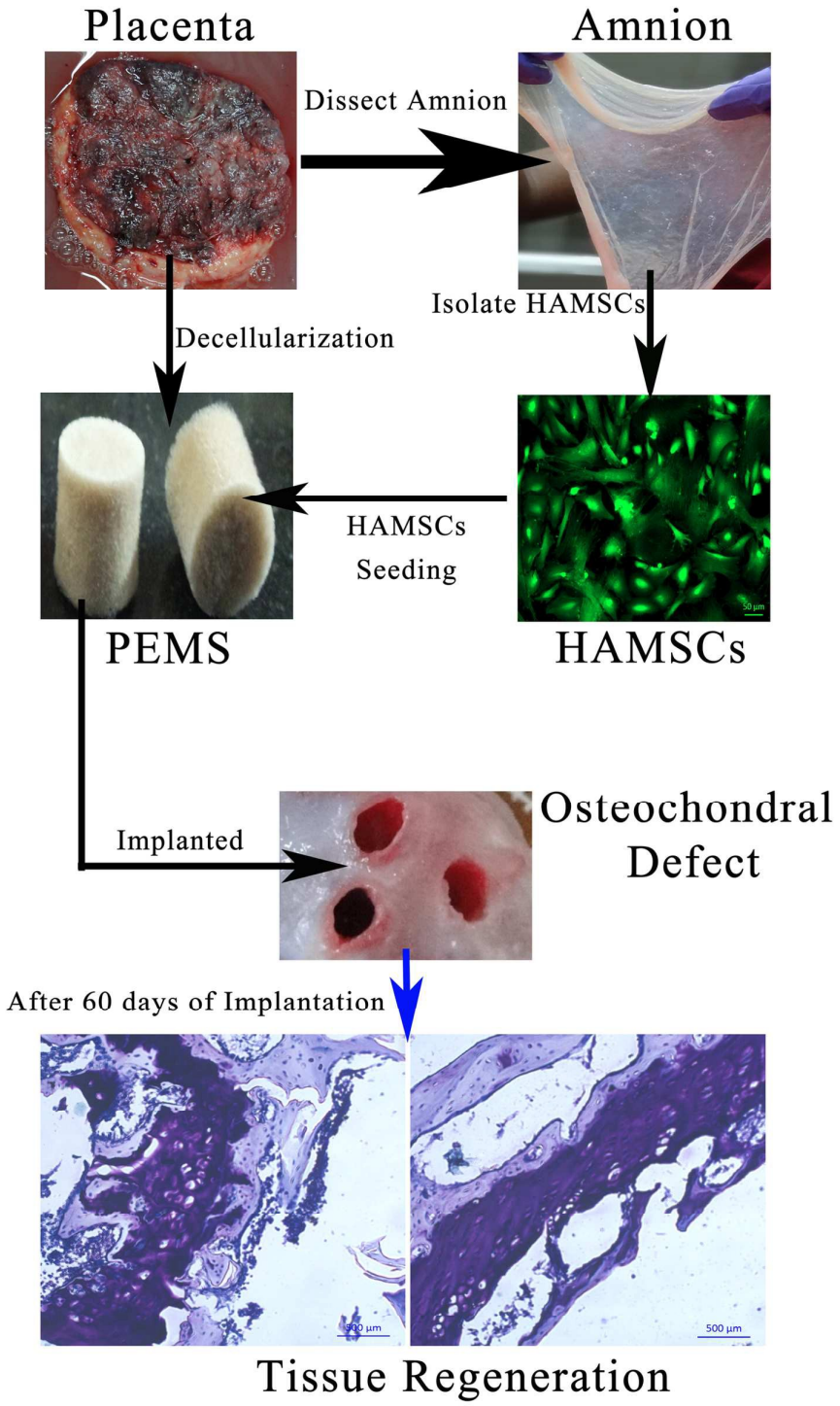

Table of contents entry graphical abstract:

Human Placental Derived Extracellular Matrix Sponges Coupled with Amniotic Membrane-Derived Stem Cells for Osteochondral Tissue Engineering

Figure

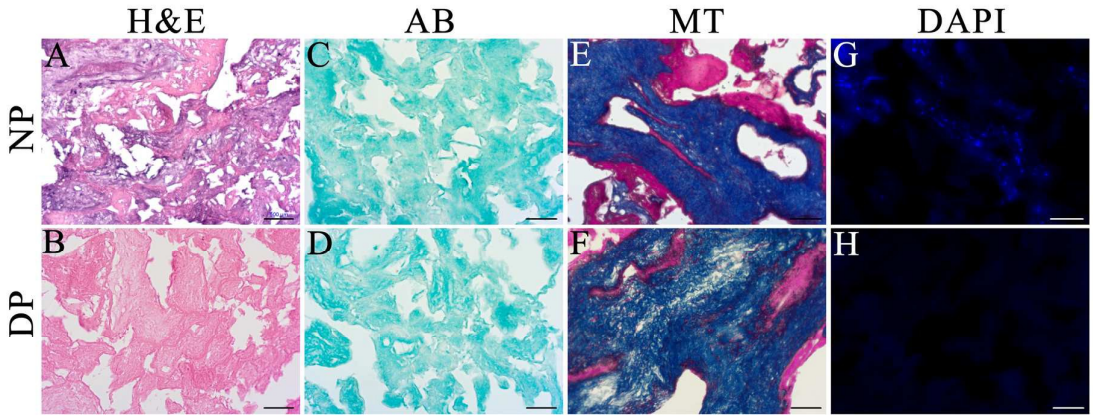

Fig. 1 H&E staining of (A) NP and (B) DP; AB staining of (C) NP and (D) DP; MT staining of (E) NP and (F) DP; DAPI staining of (G) NP and (H) DP; [H&E: Hematoxylin and eosin, AB: Alcian blue, MT: Masson's trichrome, DAPI: 4,6-diamidino-2-phenylindole. Scale bars: 500 μm]

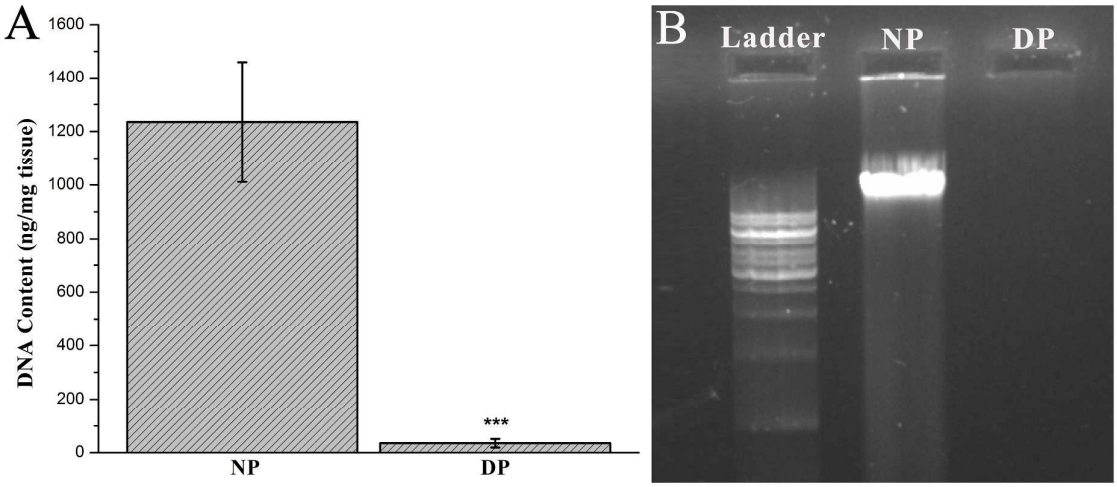

Fig. 2 (A) DNA quantification of NP and DP; (B) Agarose gel electrophoresis of the isolated DNA from NP and DP in 1% gel.

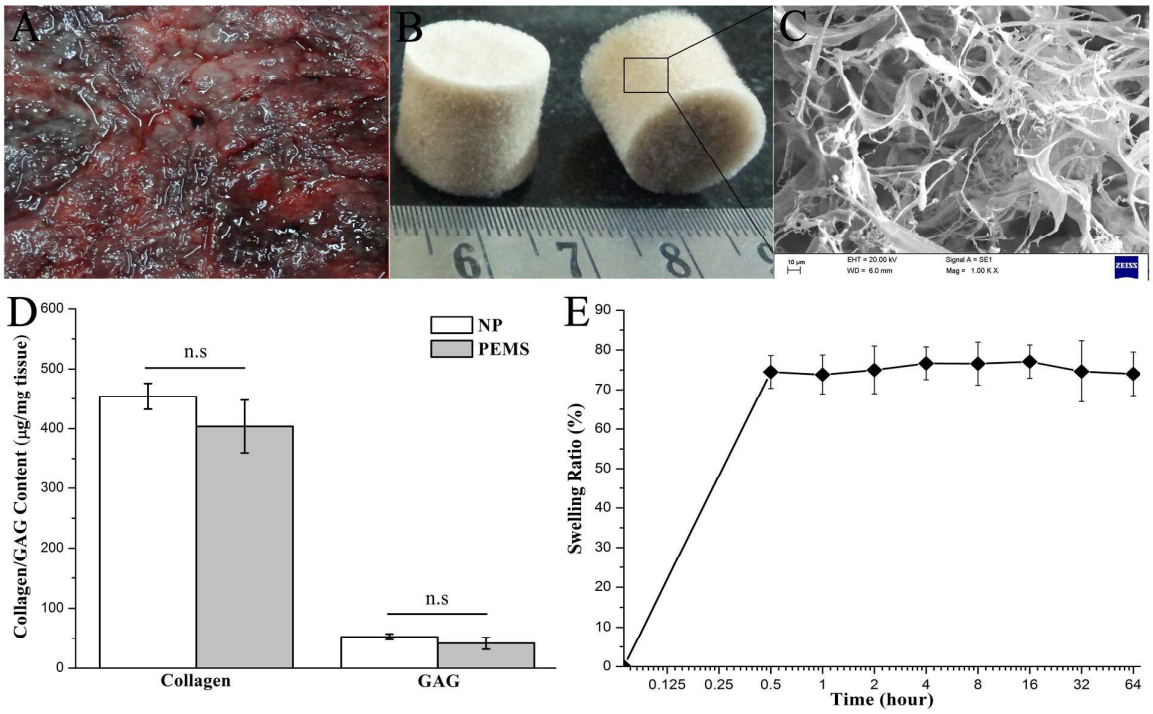

Fig. 3 (A) NP fabricated into (B) PEMS and (C) SEM micrographs of PEMS; (D) Collagen/GAG quantification of NP and PEMS; (E) Swelling kinetics of PEMS at 37 °C in PBS.

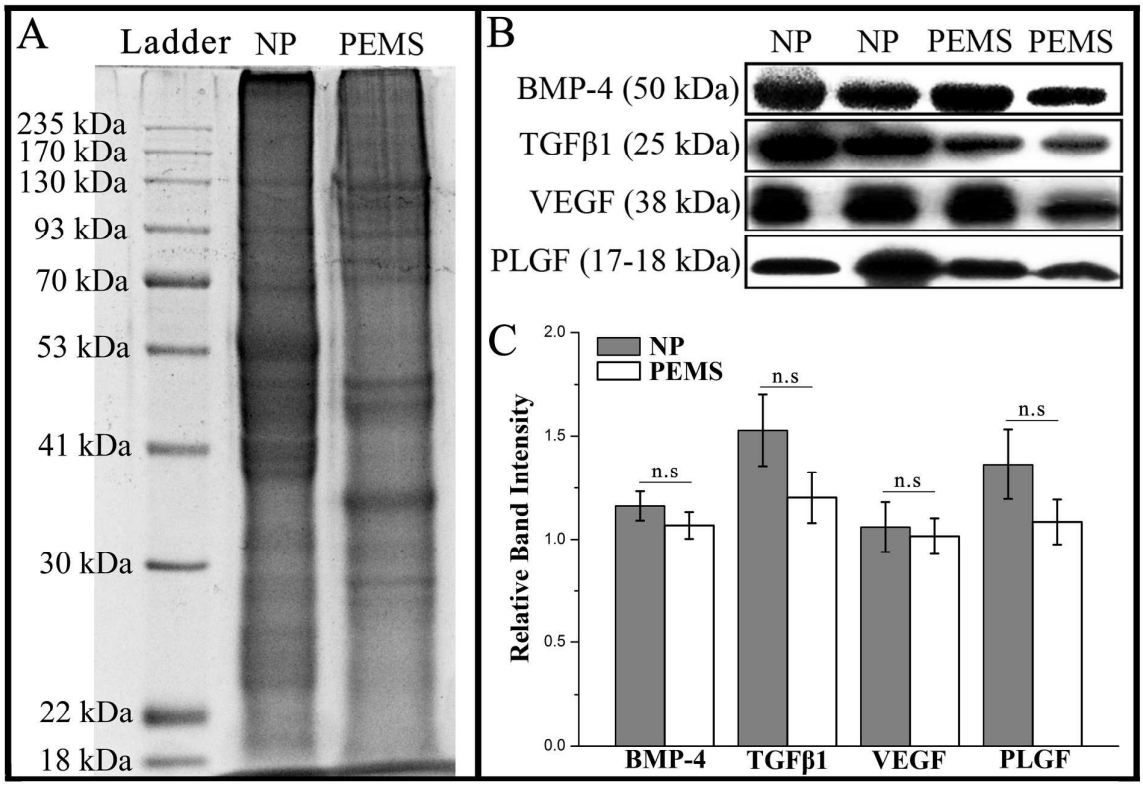

Fig. 4 (A) Total protein extracted from NP and PEMS were separated by SDS-PAGE, (B) immunoblotted using different antibodies (anti BMP-4, anti TGFβ1, anti VEGF and anti PLGF) and their respective relative band intensities.

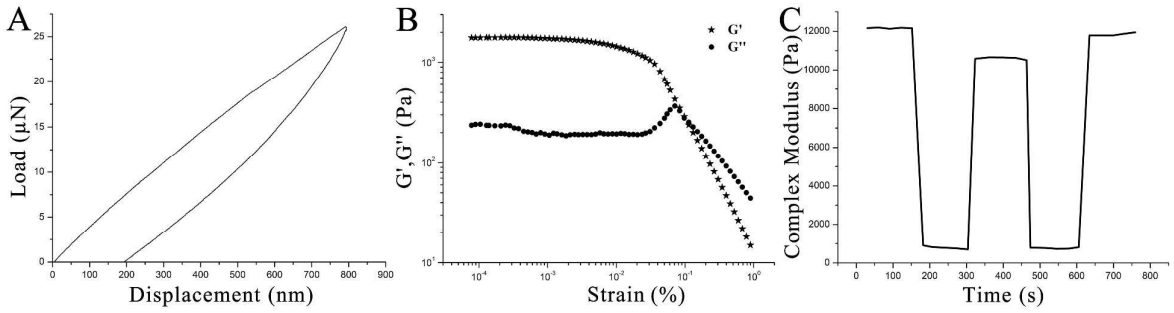

Fig. 5 (A) Representative load-displacement curve of PEMS; (B) G′, G″ of PEMS on strain sweep at constant frequency of 1 Hz; (C) Complex modulus of step-strain measurement of PEMS.

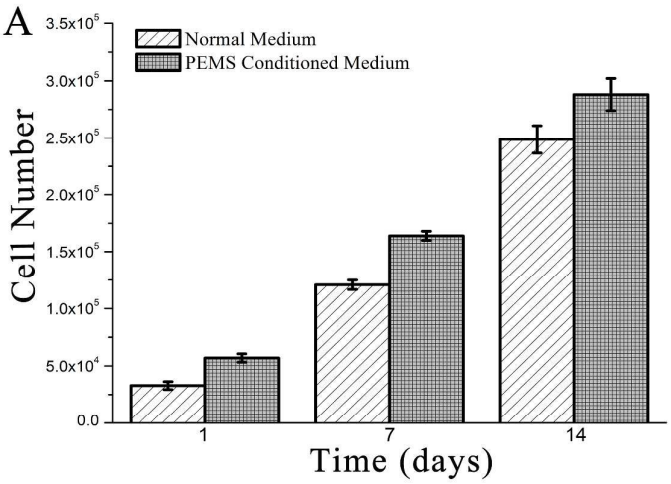

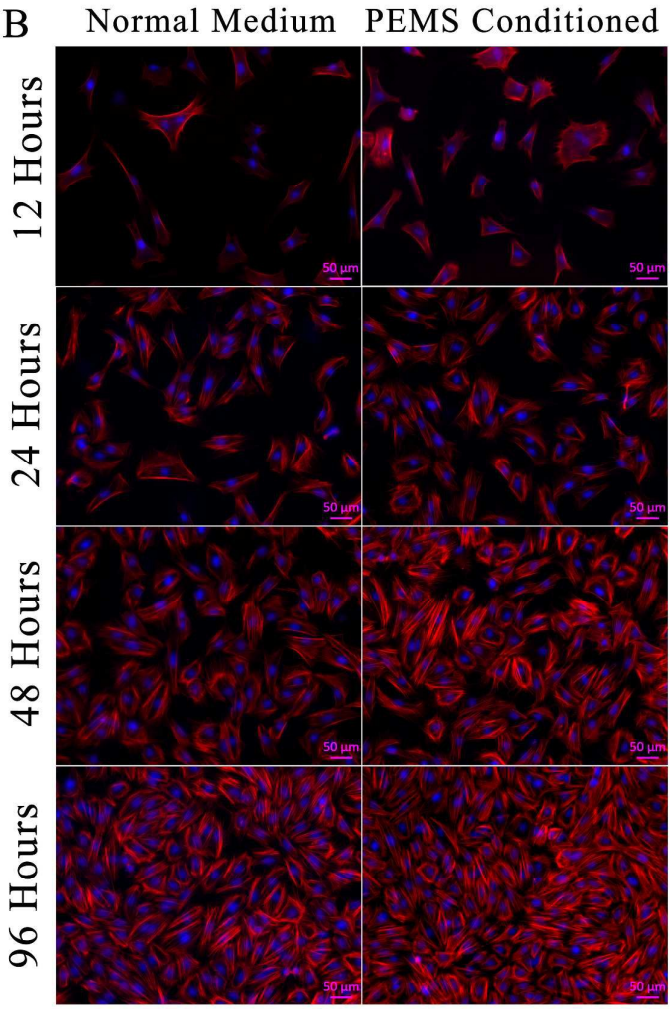

Fig. 6 Cytotoxicity analysis of PEMS. (A) Cellular metabolic activity according to MTT assay and (B) rhodamine-DAPI assay of HAMSCs cultured in PEMS conditioned and normal medium.

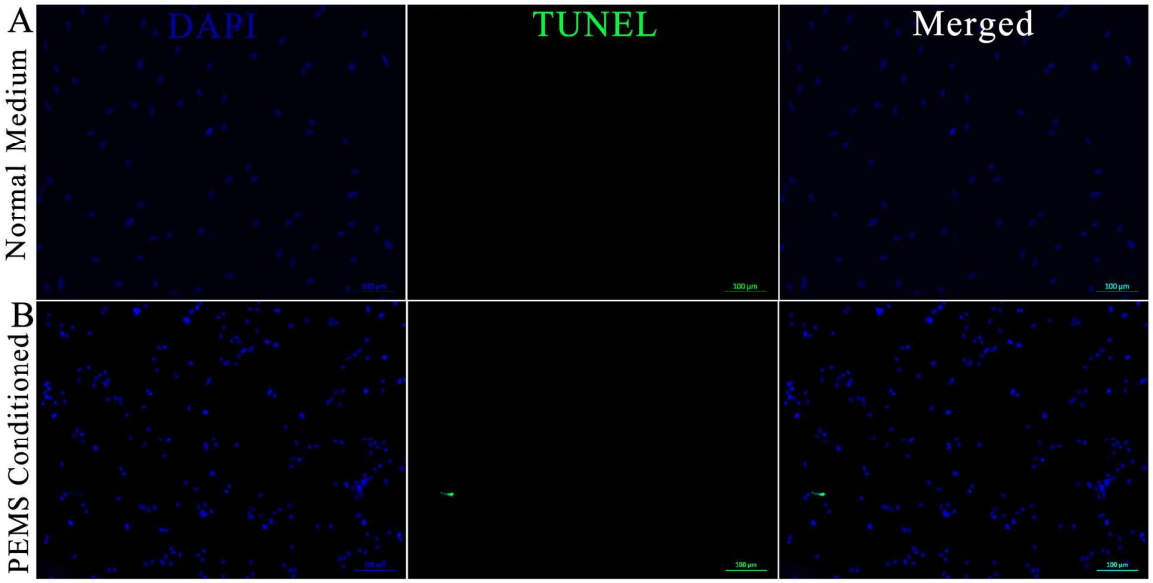

Fig. 7 TUNEL assay images after 14 days of HAMSCs cultivation in (A) normal and (B) PEMS conditioned medium.

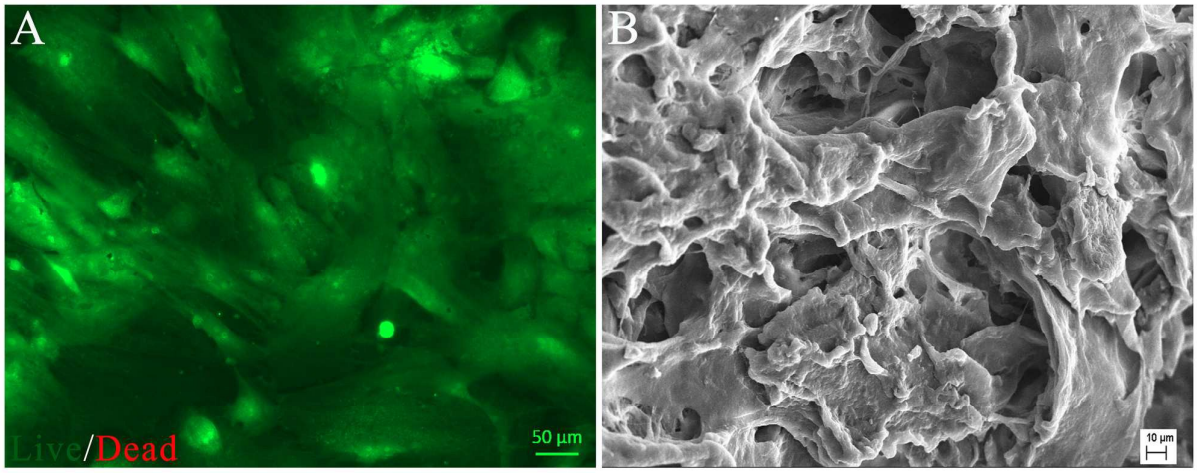

Fig. 8 Adhesion and viability of HAMSCs cultured in PEMS by (A) live-dead cell staining and (B) SEM analysis after 14 days.

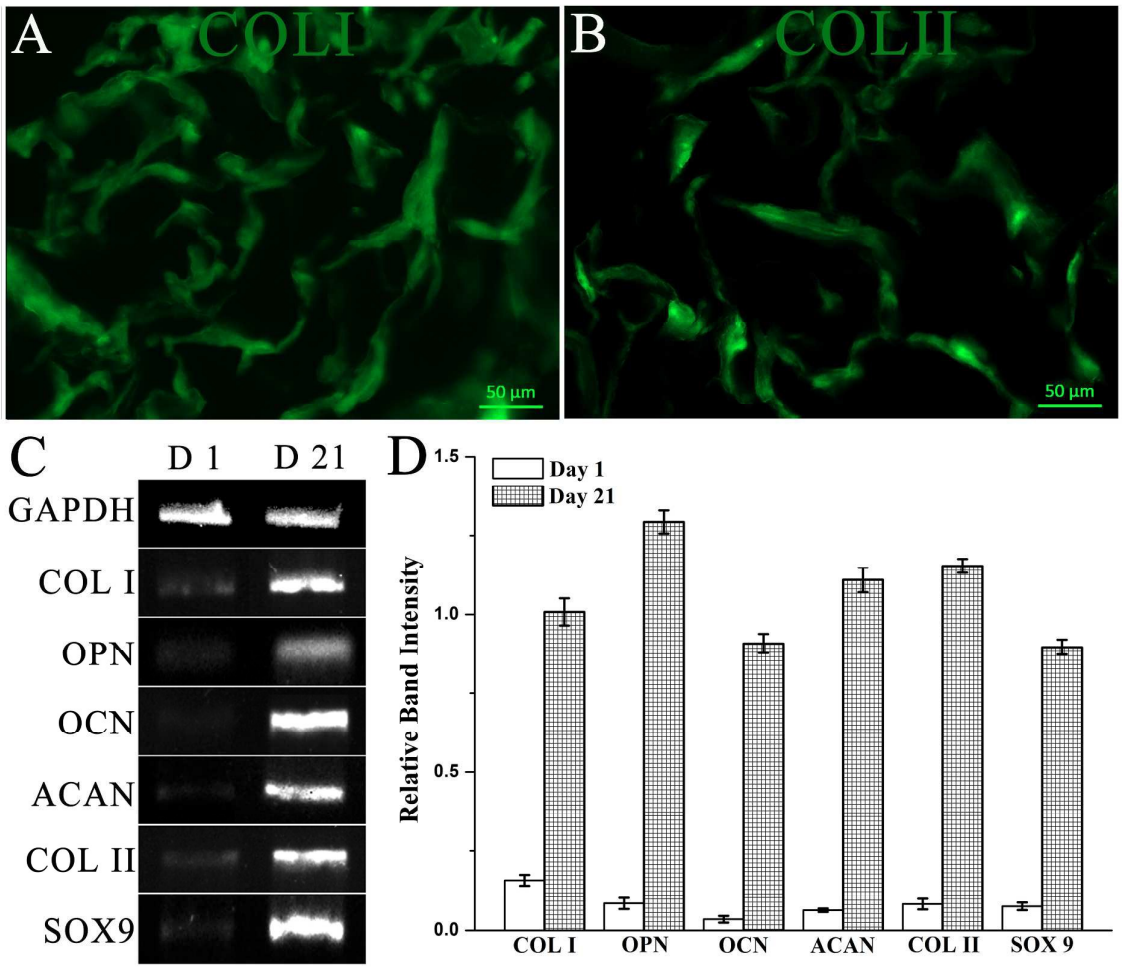

Fig. 9 Immunofluorescence images for (A) COL I and (B) COL II in PEMS; (C) RT-PCR expression profiles of osteogenic (COL I, OPN, OCN) and chondrogenic (ACAN, COL II, SOX9) related genes of HAMSCs cultured in PEMS after 1 and 21 days; (D) Their relative band intensity.

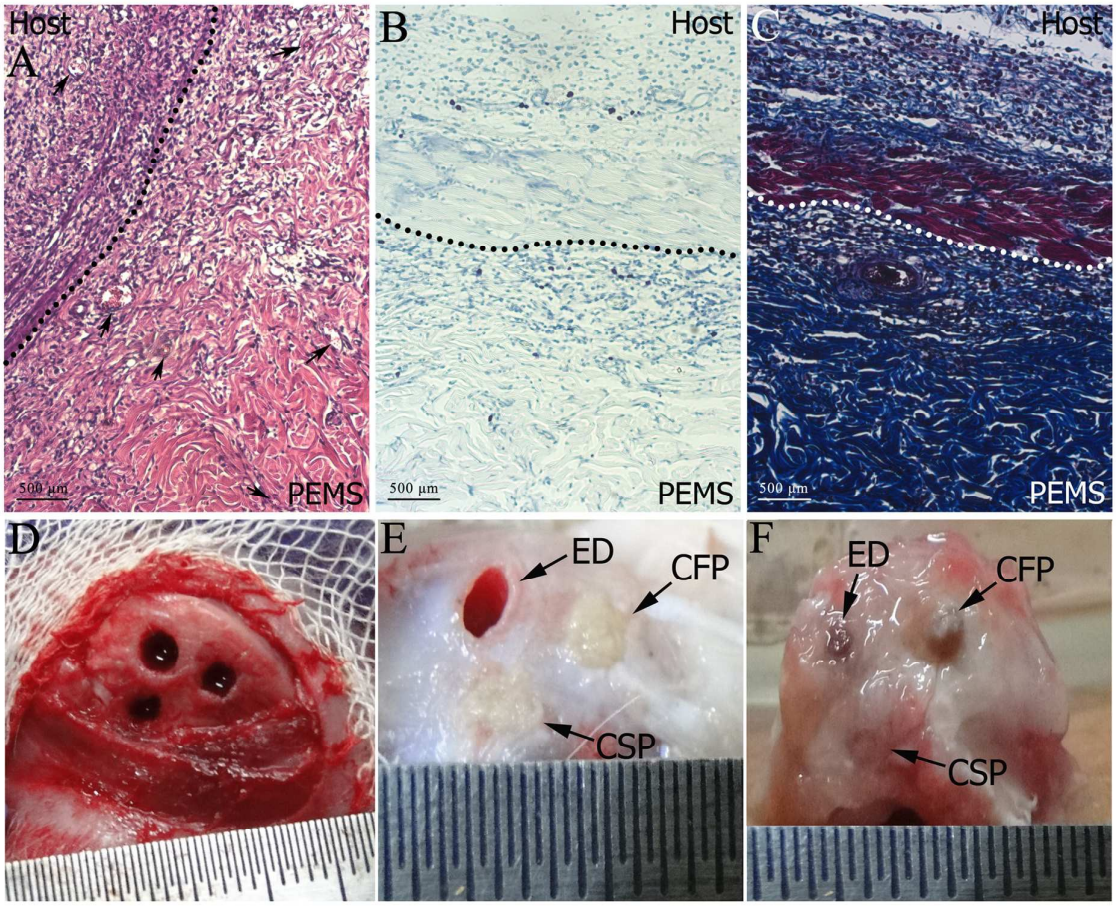

Fig. 10 (A) H&E staining of PEMS (blood vessels marked by black arrow); (B) TB staining of the PEMS; (C) MT staining of PEMS; (D) Photomicrograph of the drilled osteochondral defect sites treated with (E) CFP & CSP and (F) complete joints were retrieved after 60 days.

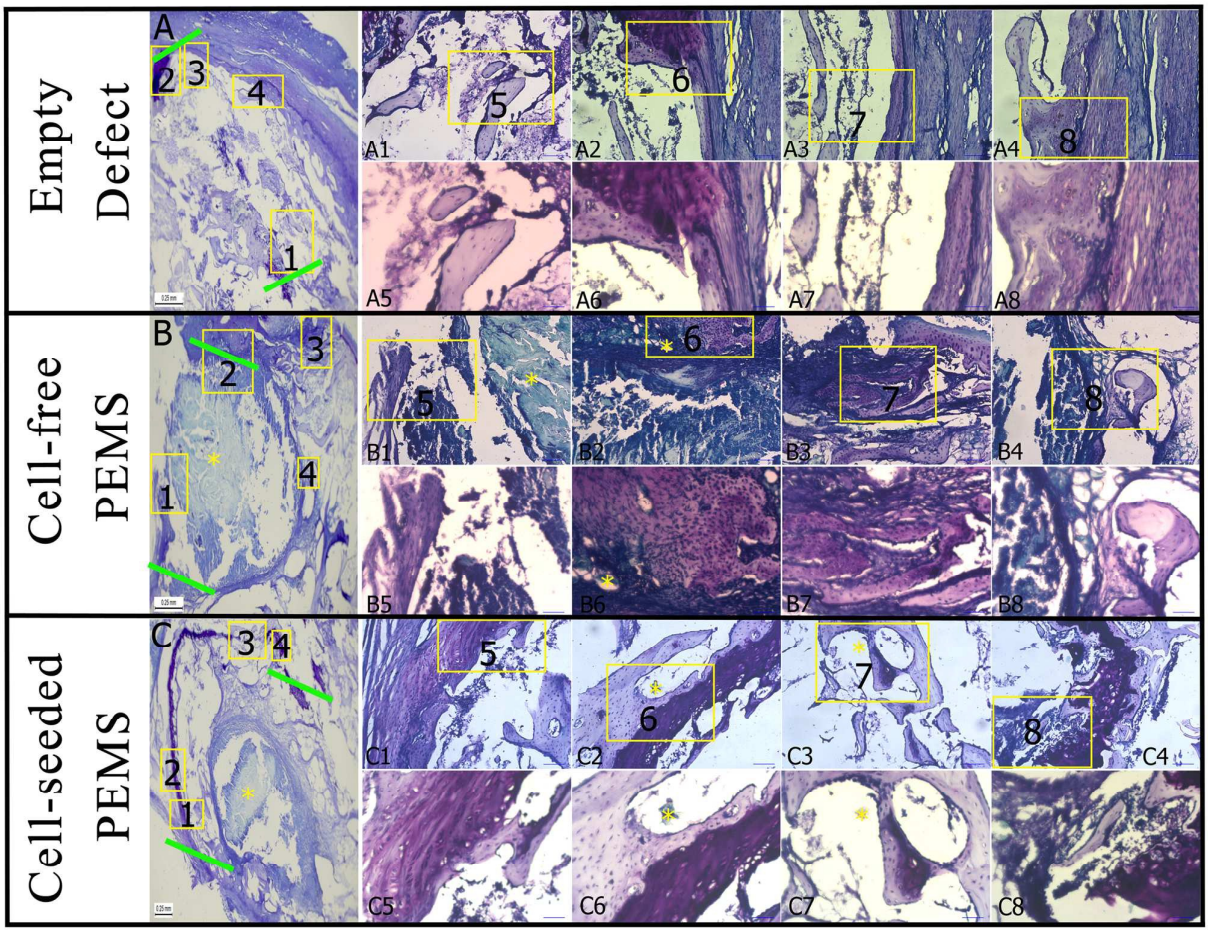

Fig. 11 Toluidine blue staining of the defects filled with CFP (B1−B8), CSP (C1−C8) and ED (A1−A8) after 60 days after surgery (green lines = defect margins; yellow stars = PEMS). Original magnification: (A1−A4, B1−B4, C1−C4) 10×, scale bar 100 μm; (A5−A8, B5−B8, C5−C8) 20×, scale bar 50 μm.

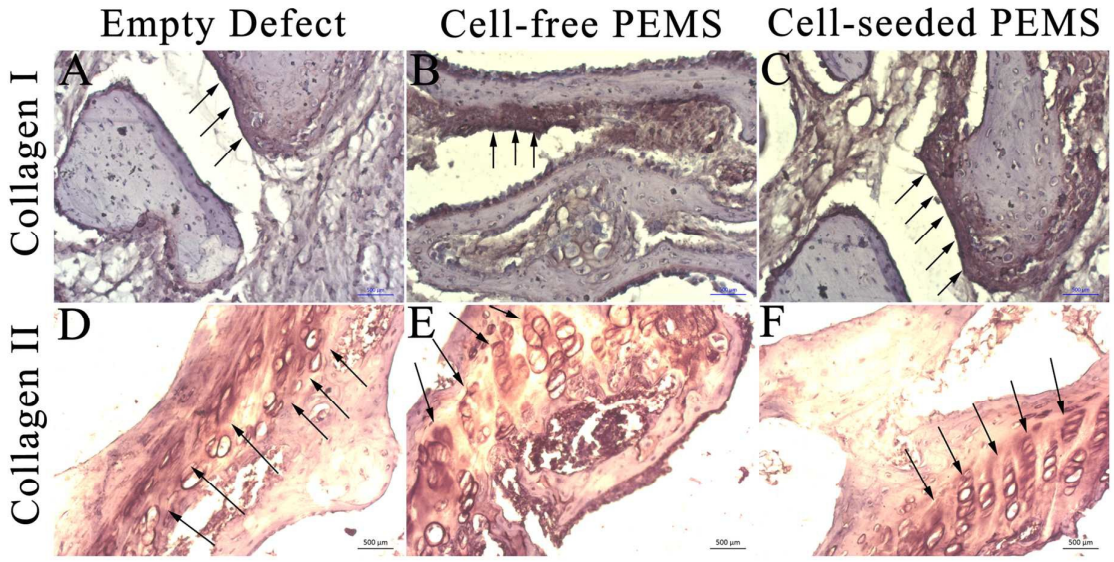

Fig. 12 Immunohistochemistry for COL I (12A−C) and COL II (12D−F) in ED, CFP and CSP (arrows points expression).